Redox Biology 27 (2019) 101191

Contents lists available at ScienceDirect

Redox Biology

journal homepage: www.elsevier.com/locate/redox

Research Paper

Voltage gated proton channels modulate mitochondrial reactive oxygen species production by complex I in renal medullary thick ascending limb

Bansari Patel[a,1], Nadezhda N. Zheleznova[b,1], Sarah C. Ray[a], Jingping Sun[a], Allen W. Cowley Jr.[b], Paul M. O'Connor[a,*]

[a] Department of Physiology, Medical College of Georgia, Augusta, Georgia, USA
[b] Department of Physiology, Medical College of Wisconsin, Milwaukee, WI, USA

A B S T R A C T

Hv1 is a voltage-gated proton channel highly expressed in immune cells where, it acts to maintain NAD(P)H oxidase activity during the respiratory burst. We have recently reported that Hv1 is expressed in cells of the medullary thick ascending limb (mTAL) of the kidney and is critical to augment reactive oxygen species (ROS) production by this segment. While Hv1 is associated with NOX2 mediated ROS production in immune cells, the source of the Hv1 dependent ROS in mTAL remains unknown. In the current study, the rate of ROS formation was quantified in freshly isolated mTAL using dihydroethidium and ethidium fluorescence. Hv1 dependent ROS production was stimulated by increasing bath osmolality and ammonium chloride (NH_4Cl) loading. Loss of either p67phox or NOX4 did not abolish the formation of ROS in mTAL. Hv1 was localized to mitochondria within mTAL, and the mitochondrial superoxide scavenger mitoTEMPOL reduced ROS formation. Rotenone significantly increased ROS formation and decreased mitochondrial membrane potential in mTAL from wild-type rats, while treatment with this inhibitor decreased ROS formation and increased mitochondrial membrane potential in mTAL from $Hv1^{-/-}$ mutant rats. These data indicate that NADPH oxidase is not the primary source of Hv1 dependent ROS production in mTAL. Rather Hv1 localizes to the mitochondria in mTAL and modulates the formation of ROS by complex I. These data provide a potential explanation for the effects of Hv1 on ROS production in cells independent of its contribution to maintenance of cell membrane potential and intracellular pH.

1. Introduction

Hv1 is a voltage-gated proton channel highly expressed in immune cells where, by limiting cellular acidification and depolarization, it acts to maintain NAD(P)H oxidase activity during the respiratory burst [1]. Since its identification, Hv1 has been found in a number of cell types outside the immune system including lung epithelial cells and spermatozoa [2]. More recently, we have reported that Hv1 is also expressed in cells of the medullary thick ascending limb (mTAL) in the kidney [3] and that in a rat model of salt-sensitive hypertension and progressive renal injury (the Dahl salt-sensitive (SS) rat), deletion of Hv1 is renal protective [4].

We have reported that Hv1 contributes to reactive oxygen species (ROS) production in mTAL [3] in response to H^+ efflux and osmotic stress. While the physiological role for Hv1 in maintaining NADPH oxidase activity during the respiratory burst is well established, the role Hv1 plays in contributing to ROS production in cells, outside phagocytic cells of the immune system remains unclear. The trans-membrane voltage threshold for opening of Hv1 can be described by $V_{THRESH-OLD} = 20\,mV–40\Delta pH$ [5]. As such, under physiological conditions, opening of the channel requires both a large outward pH gradient and significant cellular depolarization. Further, rather than by driving NADPH oxidase activity, Hv1 is thought to maintain NADPH activity at a high rate by limiting feedback inhibition of the NADPH oxidase complex by low cellular pH and depolarization of the cell membrane [1]. The cellular conditions required for Hv1 channel opening are not known to occur during normal function in most cell types and, in the absence of these conditions, the contribution of channel opening to maintenance of NADPH oxidase activity remains unclear. As such, the reported ability of Hv1 to contribute to ROS production in mTAL absent a respiratory burst remains puzzling. Understanding the mechanisms through which Hv1 contributes to cellular ROS production in thick ascending limb will likely lead to a greater understanding of the physiological role of this channel in the kidney as well as other cell types outside the immune system. The objective of the current study was to investigate the source of Hv1 dependent reactive oxygen species production in mTAL.

* Corresponding author. Department of Physiology CB2206, Augusta University, 1459 Laney Walker Blvd, Augusta, GA, 30912, USA.
E-mail address: paoconnor@augusta.edu (P.M. O'Connor).
[1] these authors contributed equally to this work.

https://doi.org/10.1016/j.redox.2019.101191
Received 4 January 2019; Received in revised form 2 April 2019; Accepted 5 April 2019
Available online 16 April 2019

2. Methods

2.1. Animals

Studies used adult male and female SS rats (12–16 weeks of age) from in house colonies and the Medical College of Wisconsin and Medical College of Georgia maintained ad libitum on water and a low salt (0.4% NaCl; AIN76A; Dyets Inc, (LS)) pellet diet since weaning. All studies were conducted in accordance with the National Institutes of Health (NIH) Guide for the Care and Use of Laboratory Animals. All of the protocols were approved in advance by the institutional animal care committee at Georgia Regents University or the Medical college of Wisconsin.

Hv1$^{-/-}$, p67phox$^{-/-}$ and NOX4$^{-/-}$ mutant Dahl salt-sensitive rats were generated on the MCW SS rat genetic background using zinc-finger nuclease technology (13, 16). Functional loss of Hv1 in this strain was previously validated using whole cell patch clamp [3]. Loss of p67phox was validated by sequencing and complete loss of production in peritoneal macrophages in response to phorbol 12-myristate 13-acetate (PMA) stimulation of the respiratory burst [6]. NOX4 deletion was previously validated by Western blot analysis [7].

2.2. Micro dissection and imaging of mTAL

Rats were anesthetized with isoflurane (2–5%) and isolation of mTAL tissue strips performed as described previously [3,8–11]. Thin tissue strips containing mTALs were placed on a glass coverslip coated with the tissue adhesive Cell-Tak (BD Biosciences) or Poly-L Lysine (Sigma, p4707; Fig. 1 only). Tissue strips containing mTALs were loaded with either dihydroethidium ((DHE), 50 mmol/L, D11347 Thermofischer) in HBSS for 1 h at room temperature (RT) or JC-1 dye (15.4 μM; T3168; Thermofischer) in HBSS for 30 min at RT. Following loading, coverslips containing mTAL were washed with HBSS and placed on a heated imaging chamber and maintained at 37 °C (RC-40, Warner Instruments), that allowed the rapid exchange of superfusion buffer, and mounted on the stage of an inverted microscope (IX81 Olympus). mTAL were visualized with a ×40 water immersion objective lens. The signal was detected using a high-resolution digital camera (Photometrics Evolve, Roper Scientific). Excitation was provided by a Sutter DG-4 175W xenon arc lamp (Sutter Instruments) that allowed high-speed excitation wavelength switching. 3 to 10 mTAL epithelial cells were selected within each tissue strip to quantify changes in fluorescent intensity of dyes using Metafluor imaging software (Universal Imaging).

DHE and ethidium (Eth) fluorescent signals were stimulated by dual-wavelength excitation at 360 nm (FF01-360/12–25; Semrock) and 520 nm (FF02-520-28-25; Semrock). A 425/30-nm (FF01425/30-25; Semrock) and a 607/36-nm (FF01-607/36-25) band-pass emission filter were used to collect DHE (excitation 360 nm/emission 425 nm) and Eth (excitation 520 nm/emission 607 nm) signals, respectively. A multi-band pass mirror was utilized to allow rapid switching between DHE and Eth signals. The rate of cellular ROS formation was determined by the change in ΔETH/ΔDHE signal ratio as previously described [3,8,10,11]. Raw signals for both Eth and DHE were normalized to 1 at time = 0 to exclude loading effects. Signals were collected at ~1 s intervals. Analysis of the Eth/DHE ratio allows the rapid detection of ROS in thick ascending limb over time, while minimizing bleaching artifact associated with measurement of a single wavelength. The utility of the ETH/DHE ratio to detect ROS in thick ascending limb tubular segments has been confirmed by the addition of ROS scavengers TEMPO and by inhibitors of NADPH oxidase (Apocynin) [12]. Further, ETH/DHE ratio is sensitive to increased ROS production via the mitochondria stimulated by DETC/methionine [13]. Data obtained using this technique are consistent with results using other detection methods, including lucigenin based assays [14].

JC-1 dye was imaged using excitation 480 nm (OCT-AT480-30 filter; Chroma Scientific) with dual emission at 535 nm (OCT-AT535-40 filter; Chroma Technology VT, USA) and 575 nm (OCT-AT575-LP; Chroma). Excitation and emission signals were separated with a dichroic beam splitter (OCT-T505LPXR; Chroma). Mitochondrial membrane potential was recorded as the ratio of the red (575 nm)/green (535 nm) emission signal. Both signals were normalized to 1 at time = 0. As such, mitochondrial depolarization was indicated by a decrease in the red/green fluorescence intensity ratio. Signals were collected at 1 s intervals.

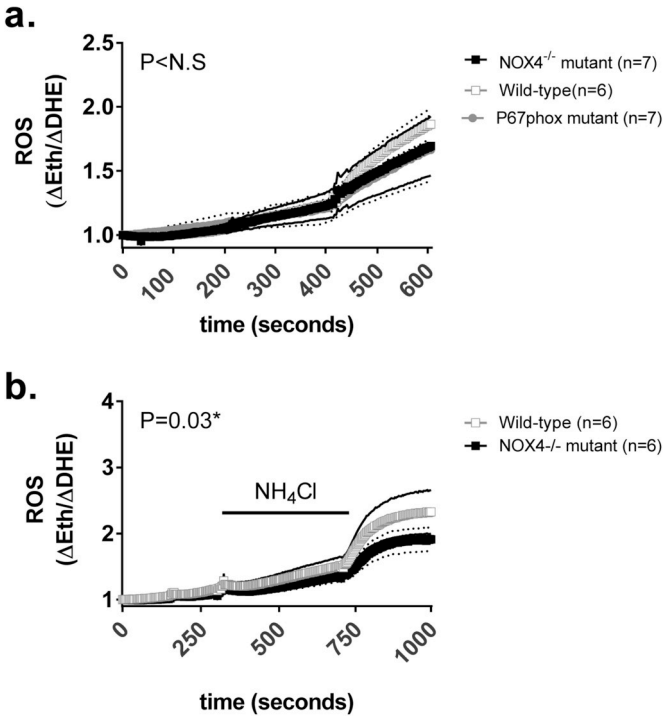

Fig. 1. ROS production in mTAL is not abolished by loss of NOX4 or p67phox Panel a), ROS production in isolated tissue strips containing medullary thick ascending limb (mTAL) from wild-type (open squares; n = 6) and p67phox$^{-/-}$ mutant (closed circles; n = 7) and NOX4$^{-/-}$ mutant rats (closed squares n = 7) loaded with the ROS sensitive dye, dihydroethidium (DHE) in response to incrementing bath NaCl concentration. 154 mM time 0–200 s, 300 mM 200–400 s and 500 mM 400–600 s. Panel b), ROS production in isolated tissue strips containing mTAL from wild-type (open squares; n = 6) and NOX4$^{-/-}$ mutant rats (closed circles n = 6) loaded with the ROS sensitive dye, DHE in response to NH_4Cl loading/removal in bicarbonate free, 0 Na^+, $BaCl_2$ media. NH_4Cl containing media was added at t = 300 s and removed at t = 600 s. X axis, time in seconds. Y axis, ROS production (ΔEth/ΔDHE) normalized to 1 at t = 0. P = results of two way repeated measures ANOVA comparing the production of ROS over time between groups. Data are expressed as mean (shapes) + SEM (thin dotted or solid lines).

2.3. Experimental protocols (tissue strips)

Animals utilized in all protocols were age and sex matched, comparing either all male or all female WT or mutant Dahl SS rats. The sex utilized for each protocol is identified in the text.

Determination of maximal Hv1 dependent ROS production in mTAL by isolating outward H^+ currents: Stimuli are needed to promote measureable ROS production in freshly isolated, non-transporting mTAL. We have previously shown that maximal ROS production in mTAL can be achieved by isolating outward H^+ currents in bicarbonate free 0 Na^+, $BaCl_2$ (100 μM) media [10] and that under these conditions ROS production is abolished in mTAL lacking Hv1[3]. As such, to investigate the molecular source of Hv1 dependent ROS production, we first examined the effect of stimulation of outward H^+ currents using NH_4Cl loading and removal in bicarbonate free 0 Na^+, $BaCl_2$ (10 mM) media on

maximal ROS production in tissue strips containing mTAL microdissected from male wild-type and NOX4$^{-/-}$ Dahl SS rats. The extracellular fluid consisted of bicarbonate free 154 mM ChCl pH 7.4 with HEPES buffer (20 mM; Sigma) and $BaCl_2$ (10 mM). The pH of the resulting solution was adjusted to 7.40 by addition of KOH/HCl. Once equilibrated at 37 °C, baseline measurements of ETH/DHE signals were recorded for 300 s before switching the bath media with the same solution containing NH_4Cl (20 mM). Recording was continued for a further 300 s before the bath solution was again exchanged with a solution identical to the original bath solution. Following the final exchange of the bath solution, Eth and DHE signals were recorded for a further 300 s. An in-line heater was utilized to minimize temperature fluctuation upon exchange of bath media (SH27-B, Warner Instruments). When NH_4Cl is added to the bath, the pH of the intracellular compartment initially increases due to the rapid inward flux of membrane permeable NH_3^+. Cells then sequester acid to return intracellular pH toward normal. The removal of NH_4Cl from the bath results in the rapid loss of NH_3^+ from the cell and subsequent intracellular acidification, which we have shown promotes Hv1 dependent ROSproduction [3,10]. The rate of ROS formation (ΔEth/ΔDHE) across the course of this protocol was compared between tissue strips isolated from male wild-type (n = 6) and male NOX4$^{-/-}$ (n = 6) Dahl salt-sensitive rats.

Stimulation of mTAL ROS production by osmotic stress: We have previously shown that osmotic stress promotes ROS production in mTAL [11]. We have utilized this stimuli to identify differences in mTAL ROS production between Dahl salt-sensitive rats and salt-resistant resistant control strains [11], and this stimuli was utilized to identify Hv1 as critical to the formation of ROS production in mTAL [15]. Given this, to investigate the molecular source of Hv1 dependent ROS production in mTAL, we investigated the incrementing bath NaCl concentration on ROS production in mTAL from male wild-type (n = 6), NOX4$^{-/-}$ (n = 7) and p67phox$^{-/-}$ (n = 7) Dahl salt-sensitive rats.

The initial bath solution consisted of Hanks' balanced salt solution at 37 °C (HBSS; Grand Island, NY) which was prepared by adding HEPES to a final concentration of 20 mM. The pH of the resulting solution was adjusted to 7.40 by addition of NaOH/HCl. Tissue strips containing TAL were imaged and Eth and DHE signals recorded for 200 s before switching the bath solution to a solution of increased osmolality achieved by the addition of 150 mM NaCl/L to the HBSS to achieve a final concentration of 300 mM. Following exchange of the bath solution signals were again recorded for a further 200 s before switching to a 500 mM solution. Eth and DHE signals were then recorded for a further 200 s.

Promotion of cellular H+ gradients in physiological medium: To determine whether cellular H^+ currents altered mTAL ROS production or mitochondrial membrane potential under physiological conditions, NH_4Cl loading/removal was performed in isolated tissue strips in physiological media (HEPES buffered (20 mM) HBSS, pH 7.40). Bath solutions were exchanged between physiological media and physiological media +30 mM NH_4Cl at 300 s and returned to physiological media at 600 s. Eth/DHE or JC-1 dye emission signals were recorded for the length of the imaging protocol (900 s total).

In addition to strain comparisons, the osmotic stress protocol, as well as the formation of cellular pH gradients in physiological media, was utilized to investigate the contribution of mitochondria to mTAL ROS production. The effect of the mitochondrial superoxide dismutase mimetic Mito TEMPOL (20 μM; n = 5) was compared to vehicle (n = 5) in 12 week old Female WT Dahl SS rats in response to increasing bath osmolality. The effect of the mitochondrial electron transport chain complex I inhibitor Rotenone (0.5 μM) vs vehicle on ROS formation in female WT (n = 5) and Hv1$^{-/-}$ (n = 5) Dahl SS rats was compared in response to both osmotic stress and following formation of cellular pH gradients in physiological media. The effect of the mitochondrial electron transport chain complex III inhibitor Antimycin A (50 μM) vs vehicle on ROS formation in male WT (n = 5) and Hv1$^{-/-}$ (n = 5) Dahl SS rats was compared in response to both osmotic stress and following formation of cellular pH gradients in physiological media.

2.4. Subcellular localization of Hv1

Male wild-type (n = 6) and Hv1$^{-/-}$ mutant (n = 6) Dahl SS rats were utilized. At 12 weeks of age 3 animals from each strain were placed on a high salt diet (8% NaCl; AIN76A; Dyets (HS)) while remaining animals were maintained on low salt (0.4%) for 2 weeks. Rats were then anesthetized with isoflurane (2–5%), the left kidney flushed with chilled saline via retrograde aortic perfusion at 4 mL/min and harvested for histology. The left kidney was immediately sliced open with a razor blade and the inner-stripe of the outer medulla removed using fine scissors. The inner-stripe of the outer-medulla was then fixed in 4% formaldehyde 0.2% glutaraldehyde in 0.1 M sodium cacodylate (NaCac) buffer, pH 7.4 for 24 h before being cut with a razor blade into approximately 1 mm cubes.

For processing for electron microscopy, tissues were dehydrated with a graded ethanol series through 95% and embedded in LR White resin (very low viscosity resin). Thin sections were cut with a diamond knife on a Leica EM UC6 ultramicrotome (Leica Microsystems, Inc, Bannockburn, IL) and collected on nickel grids. Sections were incubated in blocking buffer (Aurion blocking solution for goat gold conjugates (Aurion, Netherlands) at RT°C in a humid chamber for 2 h and with Hv1 antibody (abcam; ab117520)) diluted 1:500 in blocking buffer overnight at 4 °C. Grids were washed and incubated with anti-Rabbit nanogold (Nanoprobes, Yaphank, NY) 2–4 h at RT then washed and stained 15 min with 2% aqueous uranyl acetate. Cells were observed in a JEM 1230 transmission electron microscope (JEOL USA Inc., Peabody, MA) at 110 kV and imaged with an UltraScan 4000 CCD camera & First Light Digital Camera Controller (Gatan Inc., Pleasanton, CA).

Average mitochondrial diameter as well as the number of positive signals (clumps of gold particles (Fig. 2D) within mitochondria) were quantified from 16 + individual images containing mTAL from 2 to 3 blocks per animal. Quantification of mitochondrial diameter in each section and counting of positive signals was achieved using MetaMorph imaging software (Molecular Devices, Sunnyvale, CA). To account for non-specific signal, both LS and HS treated wild-type Dahl SS rats were compared to Hv1$^{-/-}$ rats, fed the same diet, as a negative control.

2.5. Data analysis and statistics

Where possible the identity of samples was blinded to the investigator and final values compiled after analysis. Data were analyzed using Graph pad Prism (Graph pad Inc). Fluorescent imaging data of micro-dissected mTAL were analyzed using 2-way repeated measures ANOVA and the interaction term utilized to compare treatment or strain responses over time. Immunogold staining was compared using 2 way ANOVA comparing salt diet and strain. $p < 0.05$ was considered significant.

3. Results

The rate of formation of ROS in response to incrementing osmotic stress was not different between mTAL isolated from wild-type Dahl salt-sensitive rats when compared to tubules isolated from Dahl salt-sensitive rats lacking functional p67phox or NOX4 (Fig. 1 a). Under conditions that we have found to maximally activate Hv1 dependent ROS production (0 Na media, 10 mM Ba^{2+}), ROS production in response to cellular acidification following pre-loading and then removal of NH_4Cl from the bath solution was reduced ($P < 0.03$), but not abolished in Dahl salt-sensitive rats lacking NOX4 when compared to wild-type animals (Fig. 1.b).

Functional deletion of Hv1 in Dahl salt-sensitive rats significantly ($p < 0.001$) attenuated ROS formation in freshly isolated mTAL in response to incrementing levels of osmotic stress. The greatest

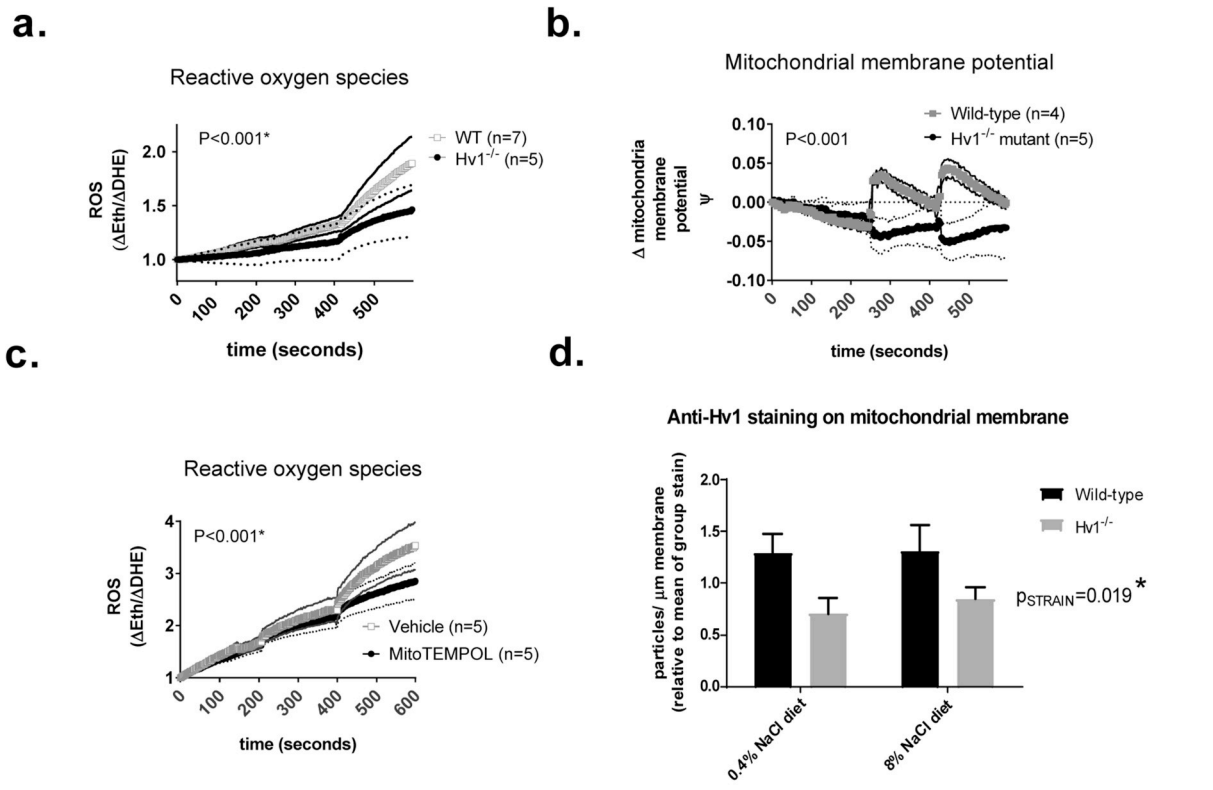

e.

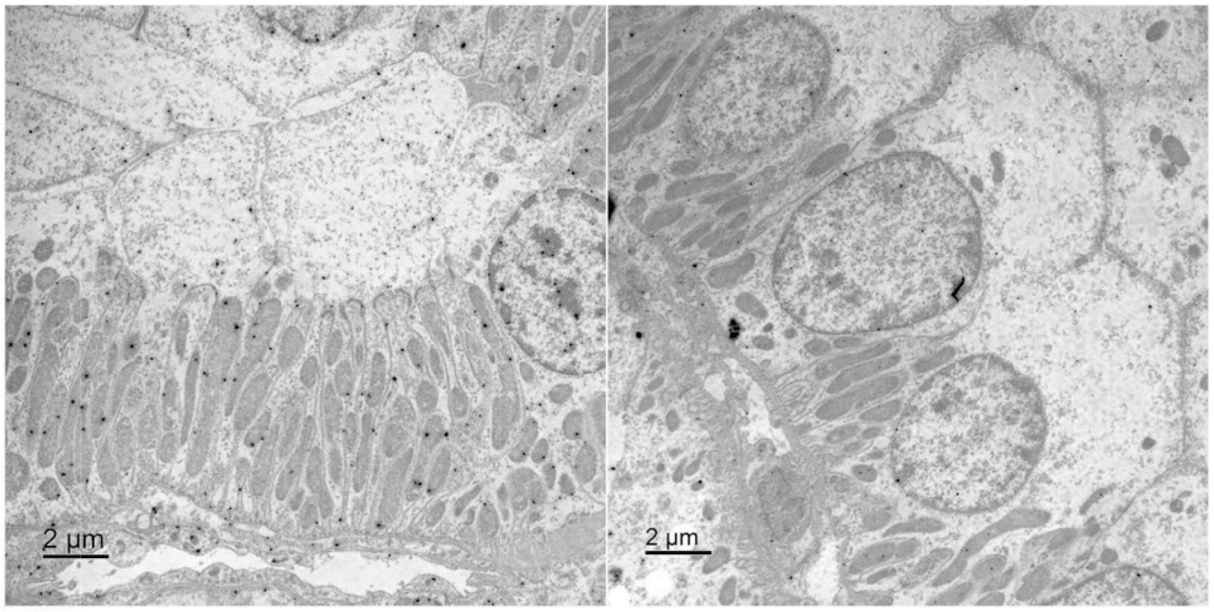

(caption on next page)

differences in the rate of ROS formation between isolated mTAL tubules from wild-type and Hv1$^{-/-}$ rats were evident at the highest bath osmolality of 500 mM NaCl (Fig. 2.a). Remarkably, in response to incrementing bath osmolality, changes in mitochondrial membrane potential measured by JC-1 dye in mTAL from rats lacking Hv1 opposed those from wild-type rats ($p < 0.001$; Fig. 2.b). In mTAL from wild-type rats, incrementing bath sodium from 154 mM to 300 mM and 300 mM–500 mM resulted in initial hyperpolarization of the mitochondrial membrane followed by a gradual recovery over the following 200 s. In difference, in mTAL from rats lacking function Hv1, incrementing bath sodium promoted a small decrease in mitochondrial membrane potential at each step (Fig. 2.b). Addition of the mitochondrial targeted ROS dismutase mimetic mitoTEMPOL (20 µM) to the bath solution significantly attenuated ROS formation in mTAL isolated from wild-type Dahl salt-sensitive rats ($P < 0.0001$). The greatest reduction in the rate of ROS formation being observed in tubules bathed in

Fig. 2. Hv1 localizes to mitochondria and Hv1 dependent ROS production to osmotic stress is blunted in wild-type Dahl SS rats by a mitochondrial ROS dismutase mimetic. Panel a); ROS production in isolated medullary thick ascending limb (mTAL) from wild-type (open squares; n = 7) and Hv1$^{-/-}$ mutant (closed circles; n = 5) rats loaded with the ROS sensitive dye, dihydroethidium in response to incrementing bath NaCl concentration. X axis, time in seconds. Y axis, ROS production (ΔEth/ΔDHE) normalized to 1 at t = 0. Panel b); mitochondrial membrane potential measured by JC-1 dye in response to incrementing bath NaCl concentration in wild-type (open squares, n = 4) and Hv1$^{-/-}$ mutant (closed circles, n = 5) rats. X axis, time in seconds. Y axis, Δmitochondrial membrane potential (red/green JC-1 fluorescence ratio) normalized to 1 at t = 0. Panel c); ROS production in isolated mTAL from vehicle treated wild-type rats (open squares; n = 5) and tubules from wild-type rats with the mitochondrial ROS dismutase mimetic MitoTEMPOL (20 μM) in the bath (closed circles; n = 5) loaded with the ROS sensitive dye, dihydroethidium in response to incrementing bath NaCl concentration. Y axis, ROS production (ΔEth/ΔDHE) normalized to 1 at t = 0. In figures a–c, bath NaCl concentration was 154 mM time 0–200 s, 300 mM 200–400 s and 500 mM 400–600 s and P = results of two way ANOVA comparing the production of ROS over time between groups. Data are expressed as mean ± SEM. Panel d); representative image of positive signal (individual clusters of gold particles) on the mitochondrial membrane. Panel e) comparison of positive Hv1 signal per total mitochondrial diameter of sections from wild-type (black columns (n = 3, each column)) and Hv1$^{-/-}$ (grey columns, n = 3 each column) Dahl salt-sensitive rats fed either a low (0.4%) or high (8%) NaCl rat chow. X axis, diet. Y axis, average particles per μM or mitochondrial membrane. P = results of two way ANOVA comparing strain. Interaction and diet were not significantly different. Data are expressed as mean (shapes) + SEM (thin dotted or solid lines).

500 mM NaCl solution (Fig. 2.c). Immuno-gold analysis of antibodies targeting Hv1 of outer-medullary sections from wild-type and Hv1$^{-/-}$ mutant Dahl salt-sensitive rats fed low (0.4%, n = 3 for each strain) and high (8%, n = 3 for each strain) sodium diets revealed sub-cellular Hv1 staining within mTAL (Fig. 2d and e). Clusters of gold particles were observed sparsely throughout the cell including along the apical membrane and within the nucleus (Fig. 2.e). In wild-type animals abundant clustering of gold particles was present within mitochondrial structures (Fig. 2.e (left panel)) and this was significantly ($p = 0.019$) greater in mitochondria from wild-type when compared to Hv1$^{-/-}$ rats. Positive signal from Hv1$^{-/-}$ rats (Fig. 2.e (right panel)) was considered to be background. 7 days of high salt feeding (8% NaCl) had no effect of the level of mitochondrial Hv1 staining in wild-type animals.

The complex 1 inhibitor rotenone (0.5 μM) had no effect on ROS formation in response to incrementing osmotic stress in mTAL isolated from wild-type of Hv1$^{-/-}$ Dahl salt-sensitive rats (Fig. 3 a, Fig. 3.b). Rotenone significantly increased the rate of ROS formation in mTAL from wild-type Dahl salt-sensitive rats in which NH_4Cl was utilized to promote an intracellular pH gradient ($p < 0.001$, Fig. 3.c). ROS formation was greater both during the alkaline and acidic periods. In contrast, rotenone significantly reduced ($p < 0.001$) ROS formation in mTAL from Hv1$^{-/-}$ rats in response to the same stimuli (Fig. 3.d). Again differences in ROS formation were present both during the alkaline and acidic phase of NH_4Cl loading. Remarkably, treatment with rotenone resulted in decreased mitochondrial membrane potential in mTAL isolated from wild-type animals (Fig. 3.e), but increased mitochondrial membrane potential in mTAL isolated from Hv1$^{-/-}$ animals (Fig. 3.f). These differences are most evident when comparing the change in initial membrane potential upon imaging (time = 0 s) between vehicle and rotenone treated tubules within animal, isolated from wild-type and Hv1$^{-/-}$ rats (Fig. 3.g; $P < 0.001$).

The complex III inhibitor Antimycin A did not alter ROS production in response to incrementing osmotic stress in mTAL from either wild-type (Fig. 4 **a**) or Hv1$^{-/-}$ (Fig. 4.b) rats. Similarly, Antimycin A had no effect to alter ROS production in mTAL from either wild-type (Fig. 4.c) or Hv1$^{-/-}$ (Fig. 4.d) rats in response to NH_4Cl loading.

4. Discussion

The major finding of the current study is that the voltage gated proton channel Hv1 modulates ROS formation in mTAL tubular segments by mitochondrial complex I. We have found that Hv1 contributes to ROS formation in mTAL [3,10]. This result has been puzzling, as it suggests that Hv1 contributes to ROS production independent of its well established role to maintain the activity of NADPH oxidase by limiting cellular acidification and depolarization [1]. The localization of Hv1 to mitochondria and demonstration that loss of this channel modulates cellular ROS formation in response to inhibition of mitochondrial complex I provides a potential explanation for these previous findings, indicating that the mitochondria rather than NADPH oxidase enzyme complexes are the primary source of Hv1 dependent ROS in mTAL. This finding is consistent with our previous observations that Amiloride analogues inhibited Hv1 dependent ROS production in mTAL [10,11]. Amiloride analogues are known to act on mitochondria to inhibit ROS formation [16,17]. A mitochondrial source of ROS may also explain our observation that alterations in intracellular Na concentration modulate Hv1 dependent ROS production in mTAL, despite Na having little reported effect on membrane bound Hv1 channel activity [3].

The mitochondria are an important source of cellular ROS production and mitochondrial ROS are critically important to both physiological and pathological cell functions. Complex I and III are generally considered the most important sites of ROS production by the electron transport chain. Rotenone, which inhibits complex I is known to promote loss of mitochondrial membrane potential and increase mitochondrial ROS production [18]. Given the importance of mitochondrial ROS production toward cellular physiology, our finding that in the absence of Hv1, inhibition of complex I with rotenone resulted in decreased rather than increased ROS production and increased mitochondrial membrane potential is striking. These data indicate that Hv1 may play a previously unrecognized, but pivotal role in modulating mitochondrial ROS production at complex I, and suggest that future investigation into the biophysical impact of mitochondrial Hv1 may shed light on the mechanisms that mediate mitochondrial ROS formation and membrane potential. The importance of Hv1 to mitochondrial ROS formation in cells other than mTAL remains unexplored.

We have previously reported that loss of Hv1 abolished ROS production in response to cellular acidification under conditions found to maximally stimulate ROS production in mTAL (bicarbonate free, 0 Na^+, $BaCl_2$ media) [3]. In the current study we first investigated the contribution of NOX4 to Hv1 dependent ROS production in mTAL as NOX4 has recently been demonstrated as a major source of ROS production in response to increasing tubular flow rate [19,20], a stimulus likely to occur following imitation of a high salt diet. We found that loss of NOX4 diminished but did not abolish ROS production in response to cellular acidification under these same experimental conditions we utilized to maximize Hv1 dependent ROS production. These data indicate that NOX4 is not the primary source of ROS production in mTAL in response to cellular acidification. Interestingly, while not abolished, ROS production in response to cellular acidification under these conditions was significantly reduced in NOX4$^{-/-}$ Dahl SS rats when compared to wild-type animals. We do not currently have an explanation for these results, although such a phenomena may be a result of interaction between two sources of cellular ROS, i.e. ROS induced ROS production [21].

Our group has demonstrated that renal oxidative stress contributes to the development of hypertension [22,23]. We and others have speculated that tubular production of ROS by NADPH oxidase may provide an important link between increased dietary sodium intake and the development of renal oxidative stress [8,9,19,20]. Our finding that the mitochondria, rather than NADPH oxidase enzyme complex's may be the primary source of Hv1 dependent ROS production in mTAL in

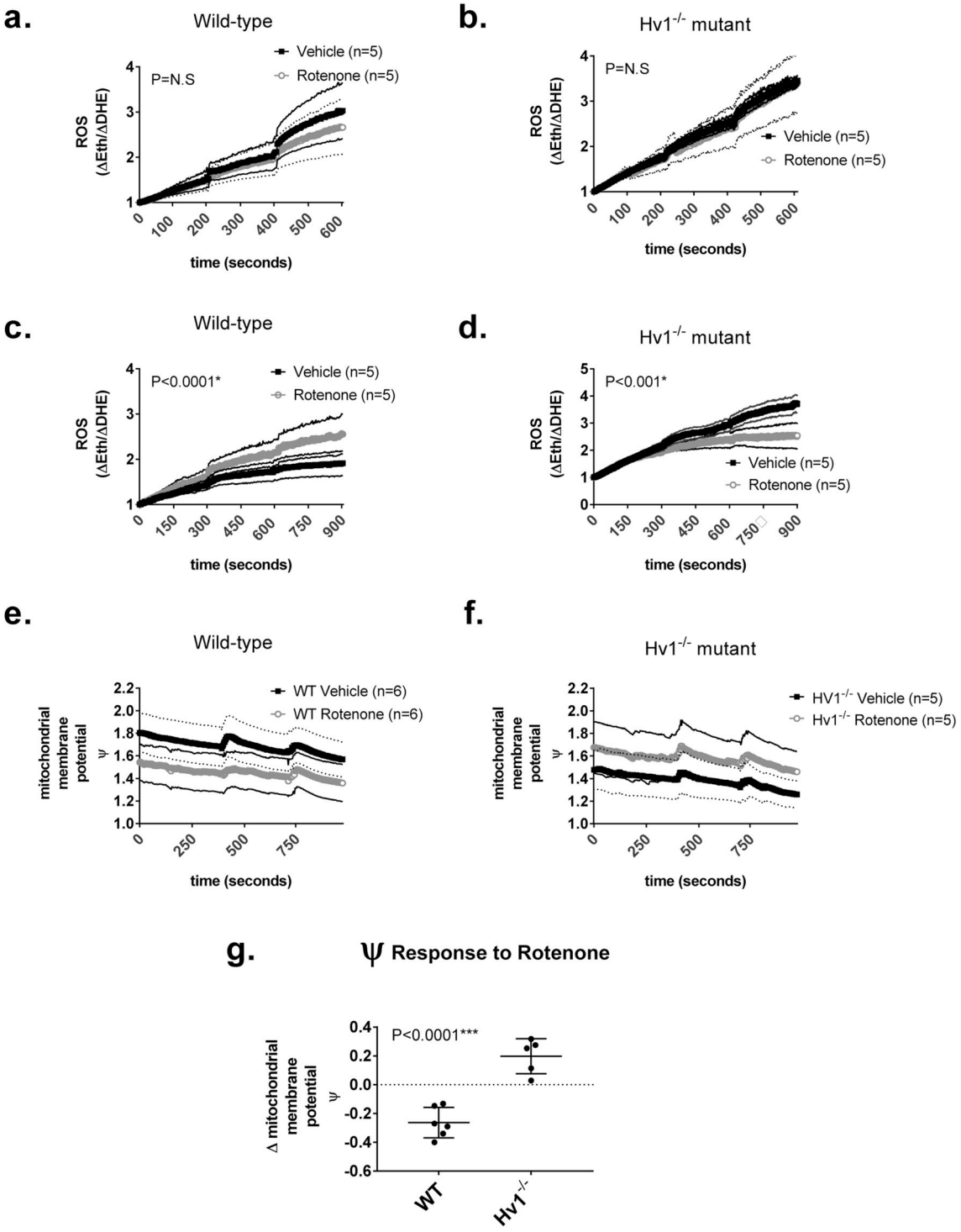

(caption on next page)

response to cellular acidification and increased osmolality is consistent with the divergent phenotypes of rats lacking Hv1 verses functional NADPH oxidase. Hv1$^{-/-}$ Dahl SS rats are protected from renal tubular interstitial injury but increases in blood pressure and proteinuria are similar to wild-type animals fed high salt [3,4]. In difference, functional deletion of either NOX4 or p67phox results in a marked reduction in the blood pressure response to salt in Dahl salt-sensitive rats [6,7]. While our study cannot exclude all potential isoforms of NADPH oxidase in mTAL, it is now clear that Hv1 dependent ROS production, which is elevated in Dahl salt-sensitive rats, is not mediated primarily by either of these two critical NADPH oxidase subunits. Given the stark differences in whole animal phenotypic responses, our data highlighting differences in cellular ROS production between rats lacking Hv1 and subunits NADPH oxidase, are likely to shed light on both the anatomical and enzymatic sources of ROS critical to the development of hypertension in the Dahl salt-sensitive rat model.

mTAL are second only to cardiac myocytes in terms of mitochondrial density [24] and mitochondrial dysfunction has been reported in the Dahl salt-sensitive rat model [25,26]. We have recently reported that functional deletion of Hv1 in the Dahl salt-sensitive rat protects

Fig. 3. The effect of the electron transport chain complex I inhibitor Rotenone of ROS production by medullary thick ascending limb (mTAL). Panel a); ROS production in isolated mTAL from vehicle treated wild-type rats (open squares; n = 5) and tubules from wild-type rats with the complex I inhibitor Rotenone (0.5 μM) in the bath (closed circles; n = 5) loaded with the ROS sensitive dye, dihydroethidium (DHE) in response to incrementing bath NaCl concentration. Panel b); as for panel a, except tubules were isolated from $Hv1^{-/-}$ mutant rats. Panel c); ROS production in isolated mTAL from vehicle treated wild-type rats (open squares; n = 5) and tubules from wild-type rats with the complex I inhibitor Rotenone (0.5 μM) in the bath (red circles; n = 5) loaded with DHE in response to cellular alkalization and acidification with NH_4Cl. The bath solution of HBSS pH 7.40 was exchanged with a bath solution containing HBSS pH 7.40 + NH_4Cl (20 mM final concentration) at time = 300 s. The bath solution was returned to the initial solution HBSS pH 7.40 without NH_4Cl at time = 600 s. Panel d); as for panel c, except tubules were isolated from $Hv1^{-/-}$ mutant rats. For panels a–d, X axis, time in seconds. Y axis, ROS production (ΔEth/ΔDHE) normalized to 1 at t = 0. Panel e); mitochondrial membrane potential measured by JC-1 dye in isolated tubules from vehicle treated wild-type rats (open squares, n = 6) and tubules from wild-type rats in response to Rotenone (0.5 μM) in the bath (closed circles; n = 6). X axis, time in seconds. Y axis, mitochondrial membrane potential (red/green JC-1 fluorescence ratio).); Panel f); mitochondrial membrane potential measured by JC-1 dye in isolated tubules from vehicle treated $Hv1^{-/-}$ mutant rats (open squares, n = 5) and tubules from $Hv1^{-/-}$ mutant rats in response to Rotenone (0.5 μM) in the bath (closed circles; n = 5). X axis, time in seconds. Y axis, mitochondrial membrane potential (red/green JC-1 fluorescence ratio). For panels a–e, P = results of two way ANOVA comparing the production of ROS over time between groups. Data are expressed as mean (shapes) + SEM (thin dotted or solid lines). Panel g); the change in initial membrane potential upon imaging (time = 0 s in panels e and f) between vehicle and rotenone treated tubules within animal, isolated from wild-type and $Hv1^{-/-}$ rats. Y axis, change in time = 0 measurement of mitochondrial membrane potential (red/green JC-1 fluorescence ratio) between vehicle and rotenone treated tubules in which the averages are shown in panels e and f. X axis, strain (wild-type or $Hv1^{-/-}$ Dahl SS rats). Data points from individual animals are shown along with mean and SEM. P = result of unpaired T-test comparing strain.

from the development of tubular interstitial fibrosis and tubular cast formation in the renal outer-medullary region where mTAL are present [4]. The contribution of Hv1 to mitochondrial dysfunction, and whether mitochondria dysfunction underlies the susceptibility of this region to injury are important questions that remain to be answered. By delineating the contribution of Hv1 to mitochondrial ROS production from NADPH oxidase dependent ROS production, this study provides an important step in understanding the contribution of different sources of ROS to renal pathology. As we have also found Hv1 to be localized to the apical membrane of mTAL, future studies will be required to differentiate the contributions of apical membrane vs mitochondrial Hv1 to renal tubular pathology in the Dahl salt-sensitive rat.

Our findings indemnify a previously unrecognized role of Hv1 in modulating mitochondrial membrane potential and ROS production. At present we can only speculate as to how the presence of Hv1 may alter ROS production by the mitochondria. Our study was not designed to determine whether Hv1 was localized to the outer or inner mitochondrial membrane. As the outer-mitochondrial membrane is reported to be highly permeable, there is little electrical potential difference between the cytosol and mitochondrial intermembrane space. Given the known biophysical characteristics of Hv1[5], localization of this channel to the outer-mitochondrial membrane may provide explanation for the seemingly low activation threshold required to observe functional effects of Hv1 in mTAL. That is, by residing on a membrane with low potential difference, mitochondrial Hv1 may open more easily than Hv1 localized to the cell membrane where membrane potential is −60 to −80mV in mTAL [15]. Both NH_4Cl loading and osmotic stress appeared to increase mitochondrial membrane potential in mTAL from wild-type animals. It is possible that Hv1 on the outer-mitochondrial membrane allows greater H^+ influx into the intermembrane space when cytosolic H^+ concentration is increased. As under normal physiological conditions, the cytosol of mTAL is relatively acidic secondary to the rapid apical reabsorption of NH_4^+, we speculate that such a mechanism allows the mitochondria to buffer decreases in cellular pH when NH_4^+ reabsorption is high. The increased mitochondrial membrane potential under these conditions may then promote greater ROS formation. It remains unclear why inhibition of complex 1 with rotenone would increase mitochondrial membrane potential in mTAL from animals lacking Hv1 and why this is associated with reduced ROS production. Further studies will be required to determine the exact location of Hv1 within the mitochondria and to determine the mechanisms through which Hv1 modulates mitochondrial membrane potential and ROS formation under various conditions. As in the current study experiments were designed to identify changes in the rate of ROS production within strains, it remains unclear if loss of Hv1 may promote greater baseline mitochondrial ROS production prior to stimulation.

Unfortunately, we have been unable to identify antibodies against Hv1 that provide a strong signal for Western blot analysis of different

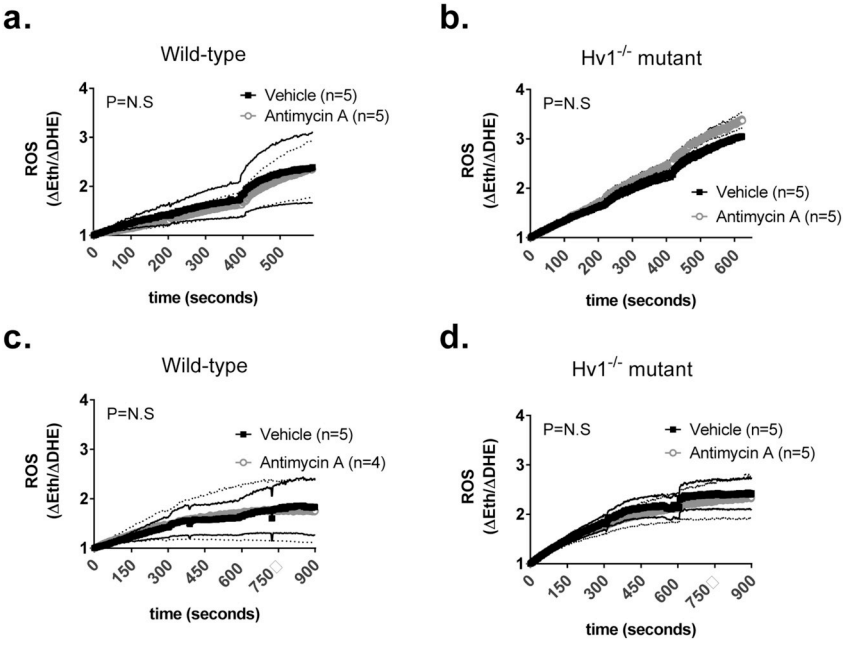

Fig. 4. The effect of the electron transport chain complex III inhibitor Antimycin A of ROS production by thick ascending limb (mTAL). Panel a); ROS production in isolated mTAL from vehicle treated wild-type rats (open squares; n = 5) and tubules from wild-type rats with the complex III inhibitor Antimycin A (50 μM) in the bath (closed circles; n = 5) loaded with the ROS sensitive dye, dihydroethidium (DHE) in response to incrementing bath NaCl concentration. Panel b); as for panel a, except tubules were isolated from $Hv1^{-/-}$ mutant rats. Panel c); ROS production in isolated mTAL from vehicle treated wild-type rats (open squares; n = 5) and tubules from wild-type rats with the complex III inhibitor Antimycin A (50 μM) in the bath (closed circles; n = 5) loaded with DHE in response to cellular alkalization and acidification with NH_4Cl. The bath solution of HBSS pH7.40 was exchanged with a bath solution containing HBSS pH 7.40 + NH_4Cl (20 mM final concentration) at time = 300 s. The bath solution was returned to the initial solution HBSS pH7.40 without NH_4Cl at time = 600 s. Panel d); as for panel c, except tubules were isolated from $Hv1^{-/-}$ mutant rats. For all figures, X axis, time in seconds. Y axis, ROS production (ΔEth/ΔDHE) normalized to 1 at t = 0. P = results of two way ANOVA comparing the production of ROS over time between groups. Data are expressed as mean (shapes) + SEM (thin dotted or solid lines).

cellar sub-fractions [3] and therefore are unable to confirm our histological data regarding the mitochondrial expression of Hv1 using this method. We are however confident in our conclusions that Hv1 is present on the mitochondria and modulates mitochondrial ROS formation and membrane potential. As quantification of membrane Hv1 was performed by individuals blinded to the source of the images and background noise was excluded by comparing positive signal with sections from $Hv1^{-/-}$ rats, we are confident that gold particles represent true Hv1. This histological data is supported by measurements of mitochondrial membrane potential demonstrating marked differences between wild-type and $Hv1^{-/-}$ rats as well as differences in cellular ROS resulting from inhibition of mitochondrial complex 1. Further, while mitoTEMPOL at the dose used in this study appeared to reduced mitochondrial membrane potential (Supplemental Fig. 1) and thus we cannot conclude that its effect is mediated entirely by superoxide scavenging, these data also point to a mitochondrial source of Hv1 dependent ROS production.

In summary, our data are the first evidence that Hv1 localizes to the mitochondria and may play an important role in modulating ROS production by complex I. These data may explain previously puzzling observations regarding the physiological impact of Hv1 in cells that do not depolarize sufficiently to open this channel at the cellular membrane, and will likely be critical to understanding the physiological role of Hv1 outside of phagocytic cells of the immune system. These data may be important in understanding the mechanisms leading to formation of ROS by the electron transport chain as well as delineating the role of mitochondrial versus NADPH oxidase derived ROS toward the development of renal pathology and salt-sensitive hypertension.

Acknowledgements

This work was supported by NIH grants to Paul O'Connor (DK099548 and 1P01HL134604) and Allen W Cowley Jr (1R01HL122662, 2P01HL116264, 1R01HL137748).

Appendix A. Supplementary data

Supplementary data to this article can be found online at https://doi.org/10.1016/j.redox.2019.101191.

References

[1] T.E. DeCoursey, The intimate and controversial relationship between voltage-gated proton channels and the phagocyte NADPH oxidase, Immunol. Rev. 273 (1) (Sep 2016) 194–218.
[2] M. Capasso, T.E. DeCoursey, M.J. Dyer, pH regulation and beyond: unanticipated functions for the voltage-gated proton channel, HVCN1, Trends Cell Biol 21 (1) (Jan 2011) 20–28.
[3] C. Jin, J. Sun, C.A. Stilphen, et al., HV1 acts as a sodium sensor and promotes superoxide production in medullary thick ascending limb of Dahl salt-sensitive rats, Hypertension 64 (3) (Sep 2014) 541–550.
[4] S.C. Ray, B. Patel, D.L. Irsik, et al., Sodium bicarbonate loading limits tubular cast formation independent of glomerular injury and proteinuria in Dahl salt-sensitive rats, Clin. Sci. (Lond). 132 (11) (Jun 15 2018) 1179–1197.
[5] T.E. DeCoursey, Voltage-gated proton channels: molecular biology, physiology, and pathophysiology of the H(V) family, Physiol. Rev. 93 (2) (Apr 2013) 599–652.
[6] D. Feng, C. Yang, A.M. Geurts, et al., Increased expression of NAD(P)H oxidase subunit p67(phox) in the renal medulla contributes to excess oxidative stress and salt-sensitive hypertension, Cell Metabol. 15 (2) (Feb 8 2012) 201–208.
[7] A.W. Cowley Jr., C. Yang, N.N. Zheleznova, et al., Evidence of the importance of Nox4 in production of hypertension in Dahl salt-sensitive rats, Hypertension 67 (2) (Feb 2015) 440–450.
[8] M. Abe, P. O'Connor, M. Kaldunski, M. Liang, R.J. Roman, A.W. Cowley Jr., Effect of sodium delivery on superoxide and nitric oxide in the medullary thick ascending limb, Am. J. Physiol. Renal. Physiol. 291 (2) (Aug 2006) F350–F357.
[9] T. Mori, P.M. O'Connor, M. Abe, A.W. Cowley Jr., Enhanced superoxide production in renal outer medulla of Dahl salt-sensitive rats reduces nitric oxide tubular-vascular cross-talk, Hypertension 49 (6) (Jun 2007) 1336–1341.
[10] P.M. O'Connor, L. Lu, M. Liang, A.W. Cowley Jr., A novel amiloride-sensitive h+ transport pathway mediates enhanced superoxide production in thick ascending limb of salt-sensitive rats, not na+/h+ exchange, Hypertension 54 (2) (Aug 2009) 248–254.
[11] P.M. O'Connor, L. Lu, C. Schreck, A.W. Cowley Jr., Enhanced amiloride-sensitive superoxide production in renal medullary thick ascending limb of Dahl salt-sensitive rats, Am. J. Physiol. Renal. Physiol. 295 (3) (Sep 2008) F726–F733.
[12] T. Mori, A.W. Cowley Jr., Angiotensin II-NAD(P)H oxidase-stimulated superoxide modifies tubulovascular nitric oxide cross-talk in renal outer medulla, Hypertension 42 (4) (2003) 588–593.
[13] T. Mori, A.W. Cowley Jr., Renal oxidative stress in medullary thick ascending limbs produced by elevated NaCl and glucose, Hypertension 43 (2) (2004) 341–346.
[14] A. Gonzalez-Vicente, J.H. Saikumar, K.J. Massey, et al., Angiotensin II stimulates superoxide production by nitric oxide synthase in thick ascending limbs, Phys. Rep. 4 (4) (2016).
[15] P.M. O'Connor, A. Guha, C.A. Stilphen, J. Sun, C. Jin, Proton channels and renal hypertensive injury: a key piece of the Dahl salt-sensitive rat puzzle? Am. J. Physiol. Regul. Integr. Comp. Physiol. 310 (8) (Apr 15 2016) R679–R690.
[16] A. Dlaskova, L. Hlavata, J. Jezek, P. Jezek, Mitochondrial Complex I superoxide production is attenuated by uncoupling, Int. J. Biochem. Cell Biol. 40 (10) (2008) 2098–2109.
[17] B.V. Alvarez, M.C. Villa-Abrille, Mitochondrial NHE1: a newly identified target to prevent heart disease, Front. Physiol. 4 (2013) 152.
[18] R. Ochi, V. Dhagia, A. Lakhkar, D. Patel, M.S. Wolin, S.A. Gupte, Rotenone-stimulated superoxide release from mitochondrial complex I acutely augments L-type Ca2+ current in A7r5 aortic smooth muscle cells, Am. J. Physiol. Heart Circ. Physiol. 310 (9) (May 1 2016) H1118–H1128.
[19] F. Saez, N.J. Hong, J.L. Garvin, NADPH oxidase 4-derived superoxide mediates flow-stimulated NKCC2 activity in thick ascending limbs, Am. J. Physiol. Renal. Physiol. 314 (5) (May 1 2018) F934–F941.
[20] N.N. Zheleznova, C. Yang, A.W. Cowley Jr., Role of Nox4 and p67phox subunit of Nox2 in ROS production in response to increased tubular flow in the mTAL of Dahl salt-sensitive rats, Am. J. Physiol. Renal. Physiol. 311 (2) (Aug 1 2016) F450–F458.
[21] S.I. Zandalinas, R. Mittler, ROS-induced ROS release in plant and animal cells, Free Radic. Biol. Med. 122 (Jul 2017) 21–27.
[22] A.W. Cowley Jr., Renal medullary oxidative stress, pressure-natriuresis, and hypertension, Hypertension 52 (5) (Nov 2008) 777–786.
[23] A. Makino, M.M. Skelton, A.P. Zou, R.J. Roman, A.W. Cowley Jr., Increased renal medullary oxidative stress produces hypertension, Hypertension 39 (2 Pt 2) (Feb 2002) 667–672.
[24] S. Abrahams, L. Greenwald, D.L. Stetson, Contribution of renal medullary mitochondrial density to urinary concentrating ability in mammals, Am. J. Physiol. 261 (3 Pt 2) (Sep 1991) R719–R726.
[25] X. He, Y. Liu, K. Usa, Z. Tian, A.W. Cowley Jr., M. Liang, Ultrastructure of mitochondria and the endoplasmic reticulum in renal tubules of Dahl salt-sensitive rats, Am. J. Physiol. Renal. Physiol. 306 (10) (May 15 2014) F1190–F1197.
[26] N.N. Zheleznova, C. Yang, R.P. Ryan, et al., Mitochondrial proteomic analysis reveals deficiencies in oxygen utilization in medullary thick ascending limb of Henle in the Dahl salt-sensitive rat, Physiol. Genom. 44 (17) (Sep 1 2012) 829–842.